THE JOURNAL OF PHYSICAL CHEMISTRY A

Article

pubs.acs.org/JPCA

Robust Magnetic Moments on Impurities in Metallic Clusters: Localized Magnetic States in Superatoms

Victor M. Medel, J. Ulises Reveles, M. Fhokrul Islam, and Shiv N. Khanna*

Department of Physics, Virginia Commonwealth University, Richmond, Virginia 23284, United States

Supporting Information

ABSTRACT: Introducing magnetic impurities into clusters of simple metals can create localized states for higher angular momentum quantum numbers (l = 2 or 3) that can breed magnetism analogous to that in virtual bound states in metallic hosts, offering a new recipe for magnetic superatoms. In this work, we demonstrate that $MnCa_n$ clusters containing 6−15 Ca atoms show a spin magnetic moment of 5.0 μ_B irrespective of the cluster size. Theoretical analysis reveals that the Mn d states hybridize only partially with superatomic states and introduce extra majority and minority d states, largely localized at the Mn site, with a large gap. Successive addition of Ca atoms introduces superatomic states of varying angular momentum that are embedded in this gap, allowing control over the stability of the motifs without altering the moment. Assemblies of such clusters can offer novel electronic features due to the formation of localized magnetic "quasibound states" in a confined nearly free electron gas.

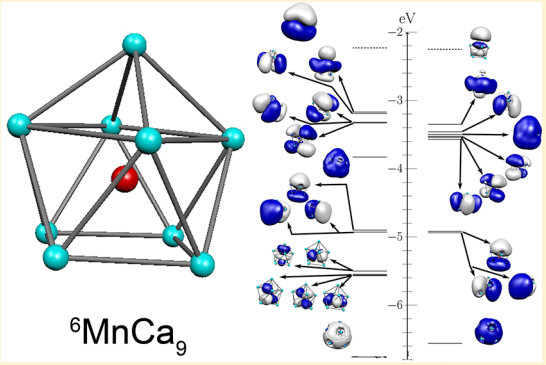

INTRODUCTION

The field of magnetic impurities in nonmagnetic metallic hosts has always attracted considerable attention because of its rich science and novel physical phenomena.[1−3] The ground states of transition-metal atoms have finite spin moments because of unpaired electrons in partially filled d levels that fill according to Hund's rule. When embedded in metallic hosts, the localized d levels interact with the conduction electron states. Almost 60 years ago Friedel argued that a resonance state could be formed that could carry a magnetic moment.[4] These "virtual bound states", broadened by the interaction with the metallic hosts, could affect transport and other properties and result in a minimum in the resistivity at low temperatures. The localized magnetic states also polarize the electron gas, introducing an oscillation in the magnetization as a function of distance, and form a many-body state that is stable at low temperatures.[5] Two interesting questions are whether similar localized magnetic states could exist at finite size and whether they could provide stable magnetic moments that survive over large variations in size. In addition, the nature of spin polarization induced by the localized impurity and how it evolves with size in finite systems are also unknown. Note also that more recent studies have focused on V, Fe, Co, and Ni impurities in alkali metal films and have reported large spin and orbital magnetic moments.[6−8]

The problem is particularly intriguing because numerous experimental and theoretical studies over the past 20 years have shown that the stability and electronic behavior of small metallic clusters can be fairly well rationalized within a model of a confined nearly free electron (CNFE) gas.[9−18]

The cluster can be modeled by a simple jellium where the positive ionic cores are replaced by a uniform positive background that is the same size as the cluster. The quantum states in such a potential collapse into a bunch of states having orbital shapes resembling those in atoms. The cluster electronic shells can be labeled as 1S, 1P, 1D, 2S, 1F, 2P, etc., where the uppercase letters are used to distinguish them from atomic orbitals, which are labeled with lowercase symbols. The cluster orbitals are distributed over multiple atoms, representing a diffuse but confined electron gas. Successive addition of electrons then leads to two distinguishing features. Unlike atoms, where partial filling of the electronic shells results in unpaired electrons following Hund's rule, the clusters can undergo atomic deformations to break degeneracy in electronic states through Jahn−Teller effects.[19] The energy gain in Jahn−Teller distortions can be greater than Hund's coupling and generally results in nonmagnetic species. Second, clusters exhibit varying stability, with species having filled electronic shells manifesting enhanced energetic stability and low reactivity. This can be seen in peaks in the mass spectrum as atoms combine to form clusters of different sizes or in reactivity with strong etchants such as oxygen.[20,21] These features have provided a conceptual basis for the superatomic state, where selected clusters classified as superatoms exhibit stable valence.[9] However, the cluster species are largely nonmagnetic.

Received: February 4, 2013
Revised: April 23, 2013
Published: April 23, 2013

One way to stabilize magnetic superatoms is to introduce transition-metal atoms that can provide localized states to breed magnetism. We recently proposed this possibility and offered VCs_8 as a possible candidate.[17] A V atom has a $3d^3 4s^2$ valence configuration, whereas a Cs atom is an alkali atom with a $6s^1$ valence state. A VCs_8 cluster has 13 valence electrons, and the ground state has a $1S^2 1P^6 1D^5$ distribution of electrons. Because the 1D state has a strong component from the atomic 3d state of V, it undergoes a large exchange splitting, leading to a cluster with a spin magnetic moment of 5.0 μ_B. In a later work, we extended the concept to include $FeMg_8$, which has 26 valence electrons.[22] The cluster had superatomic D states that hybridized strongly with Fe 3d states, leading to closed core of $1S^2 1P^6 1D^{10}$ and $2S^2$ superatom shells and a crystal-field-split $2D^4$ valence state, resulting in a magnetic moment of 4.0 μ_B. In these cases, the atomic d states hybridized with the superatomic states, and the magnetic moment changed as the relative proportion of the nonmetallic host was varied.

The key objective of the current work was to explore the possibility of a cluster that could offer a magnetic moment that is robust to variations in composition over a wide range and provide a finite-size analogue of the localized magnetic impurities in bulk simple metal hosts. The key to such an objective is to form a species in which the atomic d states do not hybridize strongly with the CNFE states and the nascent exchange splitting of the transition metal is large enough that the superatomic orbitals are positioned in the gap between the majority and minority localized 3d states. Herein, we demonstrate that $MnCa_n$ offers such a combination. Our studies of clusters containing 6−15 Ca atoms found a magnetic moment of 5.0 μ_B irrespective of the cluster size. As Ca is a divalent element, $MnCa_{15}$ has 37 valence electrons, which is a sufficient number to fill superatomic S, P, D, and even F orbitals. However, as we show, all of these states are embedded in the gap between the filled 3d majority states and unfilled 3d minority states localized at the Mn site. As we show, the evolving atomic skeleton of the Ca sites modulates the superatomic shells, including the crystal field splitting of the P and D states, without altering the overall moment. We also analyzed the polarization of the electronic cloud surrounding the Mn atom to examine the behavior of the CNFE gas in the presence of a localized magnetic moment.

METHODS

Theoretical electronic structure calculations on neutral and anionic $MnCa_n$ clusters were carried out within a first-principles density functional (DFT) framework using a gradient-corrected functional. The cluster electronic orbitals were formed from a linear combination of Gaussian-type orbitals centered at the atoms. The actual computations used deMon2k.[23,24] The exchange and correlation effects were incorporated through the functional proposed by Perdew et al.[25] A variational fitting of the Coulomb potential allowed the calculation of four-center electron repulsion integrals to be avoided.[26] Further, the exchange−correlation potential was calculated through the numerical integration of the orbital charge density. All electrons were treated explicitly using double-ζ valence plus polarization (DZVP) basis sets.[27] To facilitate the computations, the auxiliary density was expanded in primitive Hermite Gaussian functions using the GEN-A2* auxiliary function set.[28] For each cluster size, the search for the ground-state configuration was carried out by starting from several initial configurations, including spin configurations, and optimizing the geometries without symmetry constraints in delocalized internal coordinates.[29] A frequency analysis ascertained the stability of the ground state. To calculate the antiferromagnetic and ferromagnetic configurations of the $(MgCa_9)_2$ dimer as well as magnetic anisotropy, all electron calculations were carried out using the Naval Research Laboratory Molecular Orbital Library (NRLMOL) set of codes developed by Pederson and co-workers.[30−32] In NRLMOL, the Hamiltonian matrix elements are evaluated by numerical integration over a mesh of points. The basis sets, built from a variable number of primitive Gaussians, were based on a total-energy minimization for free atoms and optimized for all-electron density functional calculations.[32] The basis sets were further supplemented with a diffuse d Gaussian to allow better variational freedom. The fragment analysis was calculated using the ADF program.[33]

RESULTS AND DISCUSSION

First-principles electronic structure calculations of the ground-state atomic and electronic structure and magnetic properties of $MnCa_n$ $(6 \le n \le 15)$ clusters were undertaken to demonstrate these intriguing findings. The initial structures included previous structures for similar clusters as well as structures obtained using a genetic algorithm.

Figure 1 shows the atomic structures of $^{(2S+1)}MnCa_n$ clusters in their ground state, where $(2S + 1)$ is the spin multiplicity. As

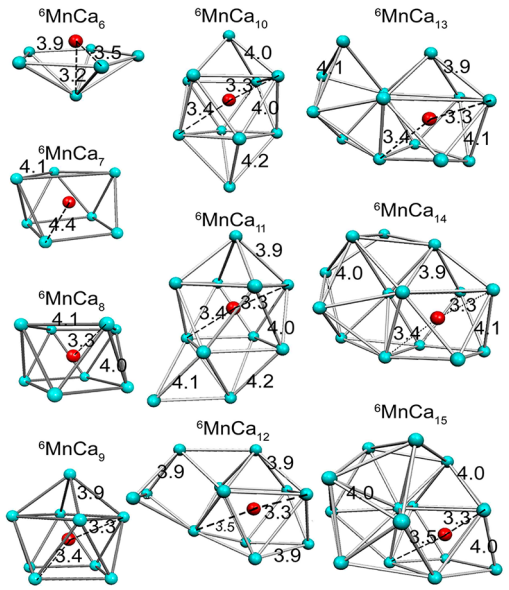

Figure 1. Ground-state $MnCa_n$ clusters $(6 \le n \le 15)$. Cyan and red spheres correspond to Ca and Mn atoms, respectively. Bond lengths are in angstroms, and superscripts indicate spin multiplicities.

Figure 1 shows, each of the clusters has a ground state with five unpaired electrons. The location of the Mn atom, however, changes with size. For $MnCa_6$, the Ca atoms form a pentagonal pyramid with Mn occupying a site above the pentagon of Ca atoms. $MnCa_7$ is the smallest cluster with an interior Mn atom. $MnCa_8$ has an interior Mn atom surrounded by a square antiprism of Ca atoms. In fact, this structure forms the skeleton for growth to larger sizes. Further addition of Ca atoms generates a $MnCa_9$ cluster with Ca decorating one of the square faces of the antiprism. This cluster has 20 delocalized valence electrons and is very stable, with a large gap between the highest occupied molecular orbital (HOMO) and the lowest

dx.doi.org/10.1021/jp4012735 | J. Phys. Chem. A 2013, 117, 4297−4303

unoccupied molecular orbital (LUMO). $MnCa_{10}$ has Ca atoms decorating both square sites of the antiprism. Note that the two Ca atoms decorating the square faces are not symmetrically positioned. Further addition of Ca atoms has Ca sites decorating the faces of the $MnCa_9$ framework, and the process continues until $MnCa_{15}$, in which six additional atoms surround the framework. One of the quantities of interest was the identification of any particularly stable species that could be looked upon as a potential building block. For this purpose, we investigated the progression in binding energy as successive Ca atoms were added. The incremental binding energy, ΔE_n, was monitored using the equation

$$\Delta E_n = \mathrm{E(Ca)} + E(\mathrm{MnCa}_{n-1}) - E(\mathrm{MnCa}_n) \quad (1)$$

where the terms $E(\mathrm{Ca})$, $E(\mathrm{MnCa}_{n-1})$, and $E(\mathrm{MnCa}_n)$ correspond to the total energies of a Ca atom, a $MnCa_{n-1}$ cluster, and a $MnCa_n$ cluster, respectively. For a cluster $MnCa_n$, ΔE_n corresponds to the gain in energy as a Ca atom is added to the preceding cluster $MnCa_{n-1}$ or the energy required to remove a Ca atom from the given cluster.

Changes in ΔE_n, defined analogously, were the hallmark of enhanced stability in the mass spectrum of pure Na_n clusters in the first identification of magic numbers. Figure 2A shows ΔE_n as a function of n, where $MnCa_8$, $MnCa_9$, $MnCa_{12}$, and $MnCa_{15}$ appear to be locally stable. In each case, the energy required to remove a Ca atom exceeds around 0.9 eV. Whereas the energetic stability represents the clusters' resistance toward fragmentation, the clusters should also be chemically stable against reactivity. As for atoms, this can be monitored through the HOMO−LUMO gap, where a large gap points to resistance of the cluster to donate or acquire charge. In fact, we previously showed that the reactivities of pure and hydrated aluminum clusters with strong etchants such as oxygen are directly related to the HOMO−LUMO gap.[21] Figure 2B shows the HOMO−LUMO gap as a function of n. The gap varies significantly with size, with $MnCa_9$ exhibiting the highest gap of 0.92 eV. The gap is fairly high, although smaller than that in Al_{13}^-, which has a gap of 1.87 eV.[34] Given its high ΔE_n, $MnCa_9$ can thus be regarded as a magic species. This observation is further reinforced by the geometry of $MnCa_{15}$, which can be described as a $MnCa_9$ unit surrounded by Ca atoms.

A single Mn atom has five unpaired electrons with an atomic configuration of $3d^54s^2$. We therefore examined the variation in the magnetic moment as successive Ca atoms were added. Figure 1 shows that all of the clusters had a spin magnetic moment of 5.0 μ_B irrespective of the cluster size. This observation is surprising, as each successive Ca contributes two electrons to the valence pool that fill the lowest unoccupied states. One would then expect a change in the magnetic moment of the resulting cluster depending on whether the extra electrons occupy majority or minority states. This is particularly puzzling because the moment remained unchanged from $MnCa_6$ to $MnCa_{15}$, which involves the addition of 18 valence electrons. Equally puzzling are the variations in the resiliency of the spin magnetic moment, defined as the energy difference between the ground state and the nearest state of different spin multiplicity. This energy, referred to as spin excitation, is shown in Figure 2C. Note that the spin excitation varies significantly with size and shows a maximum for $MnCa_9$. To identify the origin of these intriguing behaviors, we analyzed the electronic structures of these clusters. Figure 3 shows the one-electron levels and the electronic orbitals associated with each level for the spin-up and spin-down configurations for

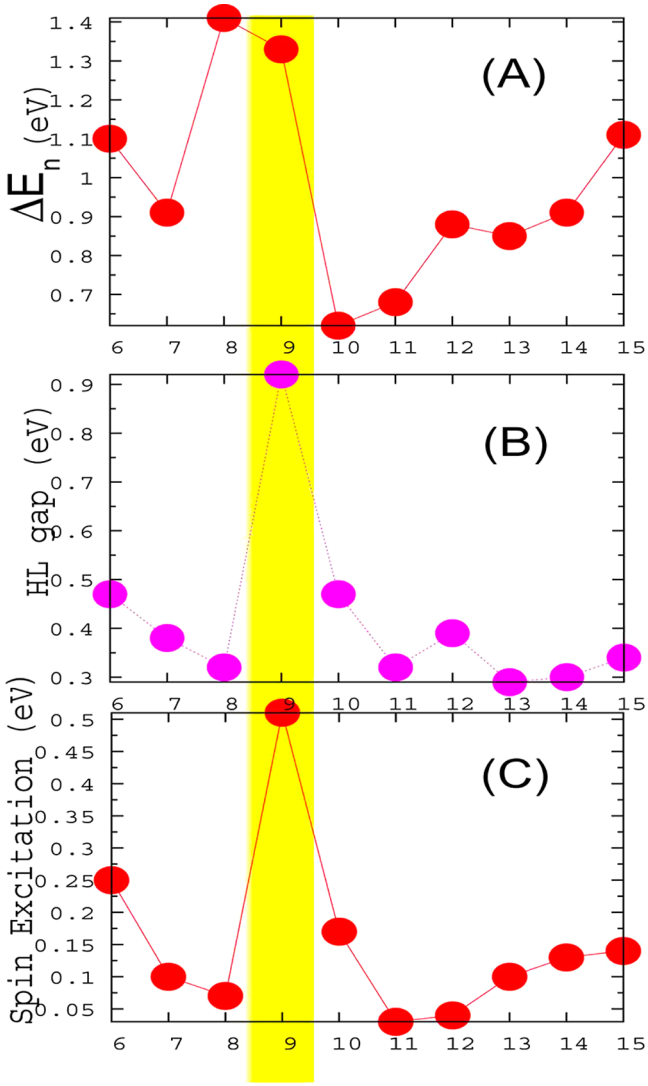

Figure 2. Variations in (A) binding energy (ΔE_n), (B) HOMO−LUMO (HL) gap, and (C) spin excitation energy for the $MnCa_n$ (n = 6−15) cluster series as functions of the number of Ca atoms.

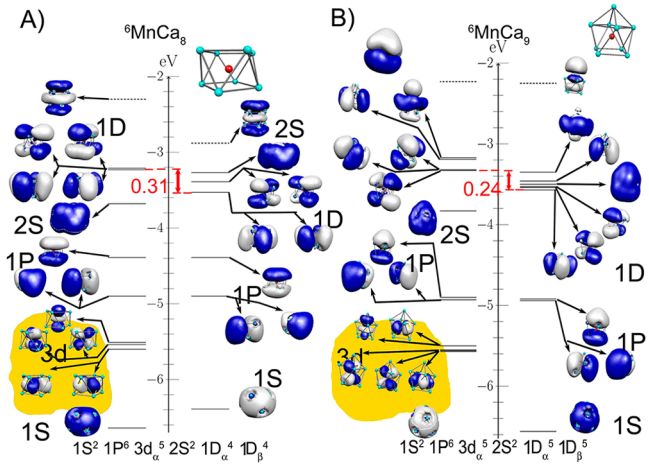

Figure 3. One-electron energy levels and molecular orbital wave function isosurfaces (isovalue = 0.01 au) for (A) $^6MnCa_8$ and (B) $^6MnCa_9$. For each level, the angular momentum of the supershells and the atomic 3d states are indicated.

dx.doi.org/10.1021/jp4012735 | J. Phys. Chem. A 2013, 117, 4297−4303

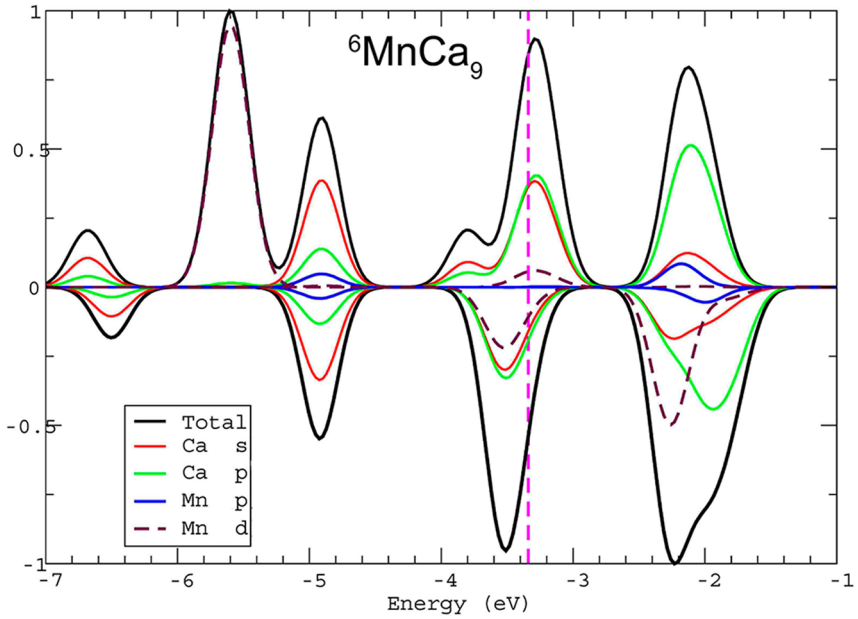

Figure 4. Density of states of ^{6}MnCa$_9$. Red and green represent the s and p contributions, respectively, of Ca atoms to the molecular states, and blue and violet represent the corresponding p and d contributions, respectively, of Mn.

^{6}MnCa$_8$ and ^{6}MnCa$_9$ clusters, and Figures S1 and S2 (Supporting Information) show the one-electron levels for ^{6}MnCa$_6$, ^{6}MnCa$_7$, ^{6}MnCa$_{10}$, ^{6}MnCa$_{11}$, ^{6}MnCa$_{12}$, ^{6}MnCa$_{13}$, ^{6}MnCa$_{14}$, and ^{6}MnCa$_{15}$. In each case, plots of the electron wave functions associated with the electronic orbitals are also shown. The global shapes of these orbitals can be used to classify them within a CNFE framework. Further, the spread of the wave functions can provide an idea about their location in the cluster.

Starting in Figure 3A with ^{6}MnCa$_8$, containing 23 valence electrons, we note the following progression of electronic states: The lowest states are 1S (α and β) orbitals distributed over the entire cluster accommodating two electrons, followed by five majority orbitals localized at the Mn ($3d_\alpha$) site. The next sets of orbitals are diffuse 1P majority and minority orbitals, again split into a two-fold degenerate pair and a single P_z orbital. Following the majority states are the 2S and two degenerate 1D orbitals, followed by another two degenerate 1D orbitals. In the minority states, after the P_z, we found the 1D orbitals, with similar degeneracies. Together, these sets of orbitals can be labeled as $1S^2 3d_\alpha^5 1P^6 1D^8 2S^2$ and fall into two groups: (1) the 3d-based majority spin (α) orbitals localized at the Mn site and (2) diffuse states of S, P, or D character distributed over the entire cluster. The localized 3d states do undergo partial mixing with superatomic 1D states that results in exchange splitting between the majority and minority 1D states. Further, the D orbitals are split into two groups: one group of four 1D orbitals and the $1D_{z^2}$ orbital. This splitting of orbitals can be looked upon as a crystal field splitting where the square antiprism structure of Ca sites can regarded as a compression of the spherical jellium in the z direction that leads to a splitting of the $1D_{z^2}$ states.[20] The Ca atom in ^{6}MnCa$_9$ occupies a site above the square face of the antiprism and removes the deformation along the z direction, and the $1D_{z^2}$ orbitals decrease in energy in a cluster having the $1S^2 3d_\alpha^5 1P^6 2S^2 1D^{10}$ shell sequence (Figure 3B). Excluding the five electrons in the localized 3d state, the ^{6}MnCa$_9$ cluster has a filled shell sequence of 20 electrons in a CNFE gas, and as shown before, the cluster is energetically stable and also has the highest HOMO−LUMO gap. ^{6}MnCa$_{10}$ is the first cluster to have F-like states (three nodes) in the cluster (Figure S1, Supporting Information). Its structure has two Ca atoms decorating the two square faces of the antiprism of Ca atoms, and the D_{z^2} orbitals drop considerably in energy. In larger clusters ($MnCa_{11}$−$MnCa_{15}$), the addition of Ca atoms leads to the filling of F-like orbitals with pairs of electrons, as shown in Figure S2 (Supporting Information).

All of the clusters from $MnCa_6$ to $MnCa_{15}$ contain 3d states localized at the Mn site, and this results in a magnetic moment of 5.0 μ_B irrespective of the size. The location of these 3d levels is also hardly changed with cluster size. An isolated Mn atom has an exchange splitting of 4.4 eV, and the unoccupied orbitals in $MnCa_9$ reveal that the minority 3d-like levels are located around 3.4 eV above the majority states. This is more clearly seen in Figure 4, which shows the density of states obtained by broadening the molecular levels by Gaussian functions with a width of 0.023 eV.

Figure 4 shows the total density of electronic states projected at the Mn and Ca sites in ^{6}MnCa$_9$. The Mn d states form a set of localized majority states around −5.6 eV, whereas the minority d states with a large Mn component are located around −2.2 eV. The 1D superatomic states located centered around −3.2 and −3.5 eV eV are primarily composed of Ca states. This is also seen from the fragment analysis of the molecular orbitals shown in Figure S3 (Supporting Information), where we have decomposed the electronic orbitals into fragments derived from Ca_9 and Mn. The overall electronic structures of the clusters can thus be regarded as a set of majority and minority 3d states localized at the Mn site and a combination of S, P, D, and F superatomic states below or in the gap between these localized states. The localized states maintain the magnetic character of the cluster, whereas the superatomic states control the overall stability by varying ΔE_n, the HOMO−LUMO gap, and the spin excitation. One can thus control the stability and magnetic character through differing

dx.doi.org/10.1021/jp4012735 | J. Phys. Chem. A 2013, 117, 4297−4303

mechanisms. The density of states at other sizes present the same picture.

For magnetic impurities in bulk metallic hosts, the impurities can introduce host polarization and form a many-body state that affects transport properties. The interaction between the localized 3d states and the CNFE gas considered here, however, presents novel features because the electron gas occupies electronic states with differing orbital character. These features originate from the parity of the localized 3d states, which allows mixing with superatomic states with compatible parity such as S and D states. The exchange splitting of the 3d atomic orbitals in Mn is consequently transmitted to S or D superatomic orbitals. This is clearly seen in Figure 3, where we consider the case of $^6MnCa_8$. The majority and minority 1S states are split by 0.24 eV, whereas the 1P states do not exhibit any splitting between majority and minority states. The 1D state also shows an exchange splitting of around 0.31 eV. One of the important issues is the evolution of this exchange coupling as the electron gas becomes more diffuse.

To quantify this progression, we calculated the difference between the majority and minority $1D_{xy}$ levels as a function of cluster size. The results are shown in Figure 5. The splitting

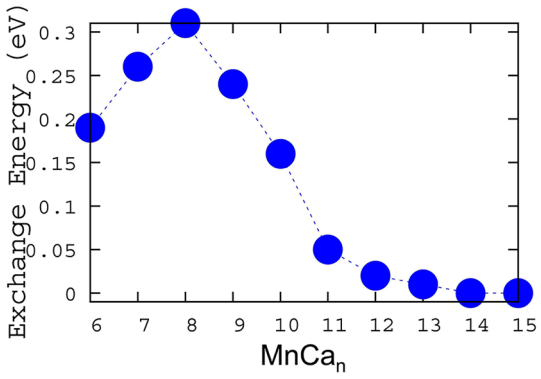

Figure 5. Exchange splitting (eV) of the majority and minority $1D_{xy}$ levels as a function of size in $^6MnCa_n$ clusters ($6 \leq n \leq 15$).

first increases and then decreases with size and is almost negligible for $^6MnCa_{15}$. Because the coupling is an indication of the effect of the localized spin moment on the electron gas, a coupled state is strong only at small sizes, and the spin polarization decreases as the superatomic orbitals become more diffuse.

A localized magnetic impurity in a bulk free electron gas induces host polarization that exhibits oscillation as a function of distance. To see any reminiscence of such a behavior at small sizes, we examined the total spin polarization in spheres of various radii centered on the Mn site. The presence of any oscillation would make the total polarization show a maximum followed by a decrease. Figure S4 (Supporting Information) shows the polarization as a function of distance for $^6MnCa_9$. The spin polarization shows a maximum around 1.7 Å followed by a decrease. It is unclear, however, whether such a minimum is unambiguously indicative of any spin oscillations in this CNFE gas.

The identification of stable magnetic species does raise the question of whether such clusters would maintain their magnetic moments when assembled to form molecules or larger clusters and how the localized moments couple in such aggregates. There are several approaches to making cluster assemblies from stable clusters. They include isolating clusters by passivating them with organic ligands,[16,35] inserting clusters into zeolite cages,[36] or depositing size-selected clusters on inert substrates.[37] Forming assemblies through direct deposition on substrates, however, requires that the magnetic properties be retained during assembly. To examine such a possibility, we investigated the evolution of the geometry and magnetic properties as two $MnCa_9$ clusters were brought together starting from large separation.

Figure 6 shows the lowest-energy structure of the composite cluster and the next higher magnetic state. The two clusters join

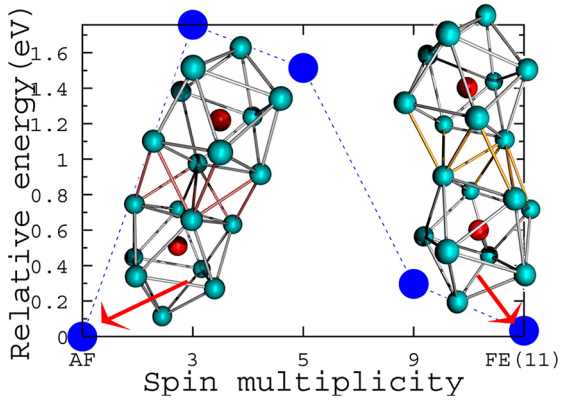

Figure 6. Relative energy (eV) of $(MnCa_9)_2$ as a function of spin multiplicity. The lowest energy is for the antiferromagnetic (AF) state with 0 μ_B, and the ferromagnetic state with 10 μ_B is 0.03 eV above the ground state.

together by sharing outer atoms but maintain their identity. Further, the ground state is antiferromagnetic with a spin magnetic moment of 0 μ_B, and the nearest energetic configuration is ferromagnetic with a spin magnetic moment of 10 μ_B. where the individual clusters, again, retain the atomic structures of the free clusters. The relative energy of the $(MnCa_9)_2$ composite cluster with different multiplicities is shown in the Figure 6, where the results indicate that the new superatoms are likely to maintain their identities upon assembly. We also examined the magnetic anisotropy in the clusters using an approach previously proposed by Pederson and Khanna.[38] Table S1 (Supporting Information) list the values calculated for the $MnCa_8$ and $MnCa_9$ clusters and for $MnCa_9$ dimers in the ferromagnetic and antiferromagnetic configurations. Note that the anisotropy of $MnCa_9$ increases upon the formation of a dimer.

To summarize, the present work opens a pragmatic approach to the design of nanoscale materials with magnetic building blocks. Such assemblies are often envisioned by using size-selected clusters, which is difficult to realize in practice. Having clusters in which the magnetic moment is maintained over a large range of compositions does not require a precise size selection of the building blocks. Because the moments are localized on the impurity sites, the magnetic features are not very sensitive to minor changes in geometry as the clusters are assembled to form larger units. This was confirmed by our preliminary studies on $(MnCa_9)_2$, which show an antiferromagnetic state or a state with a magnetic moment of 10 μ_B and further show that the clusters maintain their identity. Our previous work showed that such units have the potential for spin-polarized currents through application of small fields.[39] Although the full potential of such applications will form the

dx.doi.org/10.1021/jp4012735 | J. Phys. Chem. A 2013, 117, 4297−4303

basis of future work, as the current passes through Ca sites, the lack of spin−orbit coupling is likely to enhance spin coherence over longer distances. We hope that the present work combining magnetism and semiconducting features will stimulate experiments and further systematic searches for such species.

■ ASSOCIATED CONTENT

Supporting Information

One-electron energy levels and molecular orbital wave function isosurfaces of $^6MnCa_n$ (n = 6, 7, 10−15) (Figures S1 and S2). Decomposition of molecular orbitals of $^6MnCa_9$, into two fragments, Ca_9 and Mn (Figure S3). Polarization of $^6MnCa_9$ as a function of the distance from the Mn atom (Figure S4). Values of the magnetic anisotropy (K) for some systems (Table S1). This material is available free of charge via the Internet at http://pubs.acs.org.

■ AUTHOR INFORMATION

Corresponding Author

*Phone: (804)-828-1820. E-mail: snkhanna@vcu.edu.

Author Contributions

The manuscript was written through contributions of all authors. All authors have given approval to the final version of the manuscript.

Notes

The authors declare no competing financial interest.

■ ACKNOWLEDGMENTS

We gratefully acknowledge support from the U.S. Department of Energy (DOE) through Grant DE-FG02-11ER16213.

■ REFERENCES

(1) Gruner, G.; Zawadowski, A. Magnetic Impurities in Non-Magnetic Metals. *Rep. Prog. Phys.* **1974**, *37*, 1497−1583.

(2) van der Marel, D.; Sawatzky, G. A.; Hillebrecht, F. U. Direct Observation of the Exchange-Split Virtual Bound State in Dilute Mn Alloys. *Phys. Rev. Lett.* **1984**, *53*, 206−209.

(3) Zhuravlev, A. K.; Irkhin, V. Yu.; Katsnelson, M. I.; Lichtenstein, A. I. Kondo Resonance for Orbitally Degenerate Systems. *Phys. Rev. Lett.* **2004**, *93*, 236403-1−236403-4.

(4) Friedel, J. Metallic Alloys. *Nuovo Cimento, Suppl.* **1958**, *7*, 287−311.

(5) Kondo, J. Resistance Minimum in Dilute Magnetic Alloys. *Prog. Theor. Phys.* **1964**, *32*, 37−49.

(6) Song, F.; Bergmann, G. Strongly Enhanced Magnetic Moments of Vanadium Impurities in Thin Films of Sodium and Potassium. *Phys. Rev. Lett.* **2002**, *88*, 167202-1−167202-4.

(7) Bergmann, G.; Song, F. Electronic Transition of Vanadium Impurities in Different Alkali Hosts. *J. Magn. Magn. Mater.* **2004**, *272*, E863−E864.

(8) Gambardella, P.; Dhesi, S. S.; Gardonio, S.; Grazioli, C.; Ohresser, P.; Carbone, C. Localized Magnetic States of Fe, Co, and Ni Impurities on Alkali Metal Films. *Phys. Rev. Lett.* **2002**, *88*, 047202-1−047202-4.

(9) Khanna, S. N.; Jena, P. Atomic Clusters: Building Blocks for a Class of Solids. *Phys. Rev. B* **1995**, *51*, 13705−13716.

(10) Jena, P.; Khanna, S. N.; Rao, B. K. *Physics and Chemistry of Small Metal Clusters*; Jena, P., Khanna, S. N., Rao, B. K., Eds.; Plenum Press: New York, 1987.

(11) Brack, M. The Physics of Simple Metal Clusters: Self-Consistent Jellium Model and Semiclassical Approaches. *Rev. Mod. Phys.* **1993**, *65*, 677−732.

(12) Bergeron, D. E.; Castleman, A. W., Jr.; Morisato, T.; Khanna, S. N. Formation of $Al_{13}I^-$: Evidence for the Superhalogen Character of Al_{13}^-. *Science* **2004**, *304*, 84−87.

(13) Bergeron, D. E.; Roach, P. J.; Castleman, A. W., Jr.; Jones, N. O.; Khanna, S. N. Al Cluster Superatoms as Halogens in Polyhalides and as Alkaline Earths in Iodide Salts. *Science* **2005**, *307*, 231−235.

(14) Janssens, E.; Neukermans, S.; Lievens, P. Shells of Electrons in Metal Doped Simple Metal Clusters. *Curr. Opin. Solid State Mater. Sci.* **2004**, *8*, 185−193.

(15) Reveles, J. U.; Khanna, S. N.; Roach, P. J.; Castleman, A. W., Jr. Multiple Valence Superatoms. *Proc. Natl. Acad. Sci. U.S.A.* **2006**, *103*, 18405−18410.

(16) Hartig, J.; Stösser, A.; Hauser, P.; Schnöckel, H. A Metalloid $[Ga_{23}\{N(SiMe_3)_2\}_{11}]$ Cluster: The Jellium Model Put to Test. *Angew. Chem., Int. Ed.* **2007**, *46*, 1658−1662.

(17) Reveles, J. U.; Clayborne, P. A.; Reber, A. C.; Khanna, S. N.; Pradhan, K.; Sen, S.; Pederson, M. R. Designer Magnetic Superatoms. *Nat. Chem.* **2009**, *1*, 310−315.

(18) Li, X.; Kiran, B.; Cui, L.-F.; Wang, L.-S. Magnetic Properties in Transition-Metal-Doped Gold Clusters: $M@Au_6$ (M = Ti, V, Cr). *Phys. Rev. Lett.* **2005**, *95*, 253401-1−253401-4.

(19) Khanna, S. N.; Rao, B. K.; Jena, P. Martins, J. L. Jahn-Teller Distortion, Hund's Coupling and Metastability in Alkali Tetramers. In *Physics and Chemistry of Small Clusters*; Jena, P., Rao, B. K., Khanna, S. N., Eds.; Plenum Press: New York, 1987; p 435.

(20) Roach, P. J.; Woodward, W. H.; Hunter, W.; Reber, A. C.; Khanna, S. N.; Castleman, A. W., Jr. Crystal Field Effects on the Reactivity of Aluminum−Copper Cluster Anions. *Phys. Rev. B* **2010**, *81*, 195404-1−195404-5.

(21) Reber, A. C.; Khanna, S. N.; Roach, P. J.; Woodward, W. H.; Castleman, A. W., Jr. Spin Accommodation and Reactivity of Aluminum Based Clusters with O_2. *J. Am. Chem. Soc.* **2007**, *129*, 16098−16101.

(22) Medel, V. M.; Reveles, J. U.; Khanna, S. N.; Chauhanb, V.; Sen, P.; Castleman, A. W., Jr. Hund's Rule in Superatoms with Transition Metal Impurities. *Proc. Natl. Acad. Sci. U.S.A.* **2011**, *108*, 10062−10066.

(23) Geudtner, G.; Calaminici, P.; Carmona-Espindola, J. M.; del Campo, J. M.; Dominguez-Soria, V. D.; Flores-Moreno, R.; Gamboa, G. U.; Goursot, A.; Koster, A. M.; Reveles, J. U.; Tzonka, M.; Vasquez-Perez, J. M.; Vela, A.; Zuninga-Gutierrez, B.; Salahub, D. R. deMon2k. *WIREs Comput. Mol. Sci.* **2012**, *2*, 548−555.

(24) Koster, A. M.; Calaminici, P.; Casida, M. E.; Flores-Moreno, R.; Geudtner, G.; Goursot, A.; Heine, T.; Ipatov, A.; Janetzko, F.; del Campo, J. M.; Patchkovskii, S.; Reveles, J. U.; Salahub, D. R.; Vela, A. *deMon2k*, version 2.3.6; The deMon Developers Community: Cinvestav, México, 2006; available at www.deMon-software.com.

(25) Perdew, J. P.; Burke, K.; Enzerhof, M. Generalized Gradient Approximation Made Simple. *Phys. Rev. Lett.* **1996**, *77*, 3865−3868.

(26) Dunlap, B. I.; Connolly, J. W. D.; Sabin, J. R. On Some Approximations in Applications of Xα Theory. *J. Chem. Phys.* **1979**, *71*, 3396−3402.

(27) Godbout, N.; Salahub, D. R.; Andzelm, J.; Wimmer, E. Optimization of Gaussian-Type Basis Sets for Local Spin Density Functional Calculations. Part I. Boron through Neon, Optimization Technique and Validation. *Can. J. Chem.* **1992**, *70*, 560−571.

(28) Calaminici, P.; Janetzko, F.; Köster, A. M.; Mejia-Olvera, R.; Zuniga-Gutierrez, B. Density Functional Theory Optimized Basis Sets for Gradient Corrected Functionals: 3d Transition Metal Systems. *J. Chem. Phys.* **2007**, *126*, 044108-1−044108-10.

(29) Reveles, J. U.; Köster, A. M. Geometry Optimization in Density Functional Methods. *J. Comput. Chem.* **2004**, *25*, 1109−1116.

(30) Pederson, M. R.; Jackson, K. A. Variational Mesh for Quantum-Mechanical Simulations. *Phys. Rev. B* **1990**, *41*, 7453−7451.

(31) Jackson, K.; Pederson, M. R. Accurate Forces in a Local-Orbital Approach to the Local-Density Approximation. *Phys. Rev. B* **1990**, *42*, 3276−3281.

(32) Porezag, D.; Pederson, M. R. Optimization of Gaussian Basis Sets for Density-Functional Calculations. *Phys. Rev. A* **1999**, *60*, 2840−2847.
(33) *ADF 2012*; Scientific Computing & Modelling NV, Theoretical Chemistry, Vrije Universiteit: Amsterdam, The Netherlands, 2012; available at www.scm.com.
(34) Castleman, A. W., Jr.; Khanna, S. N. Clusters, Superatoms, and Building Blocks of New Materials. *J. Phys. Chem. C* **2009**, *113*, 2664−2675.
(35) Jadzinsky, P. D.; Calero, G.; Ackerson, C. J.; Bushnell, D. A.; Kornberg, R. D. Structure of a Thiol Monolayer-Protected Gold Nanoparticle at 1.1 Å Resolution. *Science* **2007**, *318*, 430−433.
(36) Mikhailov, M. N.; Kustov, L. M.; Kazansky, V. B. The State and Reactivity of Pt_6 Particles in ZSM-5 Zeolite. *Catal. Lett.* **2008**, *120*, 8−13.
(37) Perez, A.; Melinon, P.; Dupuis, V.; Jensen, P.; Prevel, B.; Tuaillon, J.; Bardotti, L.; Martet, C.; Treilleux, M.; Broyer, M.; Pellarin, M.; Vaille, J. L.; Palpant, B.; Lerme, J. Cluster Assembled Materials: A Novel Class of Nanostructured Solids with Original Structures and Properties. *J. Phys. D: Appl. Phys.* **1997**, *30*, 709−721.
(38) Pederson, M. R.; Khanna, S. N. Magnetic Anisotropy Barrier for Spin Tunneling in $Mn_{12}O_{12}$ Molecules. *Phys. Rev. B* **1999**, *60*, 9566-1−9566-7.
(39) He, H.; Pandey, R.; Reveles, J. U.; Khanna, S. N.; Karna, S. S. Highly Efficient (Cs_8V) Superatom-Based Spin-Polarizer. *Appl. Phys. Lett.* **2009**, *95*, 192104-1−192104-3.